Acta Crystallographica Section D
Biological Crystallography
ISSN 0907-4449

Effect of crystal freezing and small-molecule binding on internal cavity size in a large protein: X-ray and docking studies of lipoxygenase at ambient and low temperature at 2.0 Å resolution

E. Skrzypczak-Jankun,[a]*
O. Y. Borbulevych,[a]‡
M. I. Zavodszky,[b]
M. R. Baranski,[c]
K. Padmanabhan,[b]
V. Petricek[d] and J. Jankun[a]

[a]Urology Research Center, Medical University of Ohio, Toledo, OH 43614, USA, [b]Department of Biochemistry and Molecular Biology, Michigan State University, East Lansing, MI 48824, USA, [c]Lyman Briggs School of Science, Michigan State University, East Lansing, MI 48824, USA, and [d]Department of Structures and Bonding, Institute of Physics, Academy of Sciences of the Czech Republic, 180 40 Praha 8, Czech Republic

‡ Current address: Department of Chemistry and Biochemistry, University of Notre Dame, Notre Dame, IN 46556, USA.

Correspondence e-mail: eskrzypczak@meduohio.edu

Received 15 February 2006
Accepted 8 May 2006

PDB References: soybean lipoxygenase, ambient temperature, 1rrh, r1rrhsf; 93 K, 1rrl, r1rrlsf.

Flash-freezing is a technique that is commonly used nowadays to collect diffraction data for X-ray structural analysis. It can affect both the crystal and molecular structure and the molecule's surface, as well as the internal cavities. X-ray structural data often serve as a template for the protein receptor in docking calculations. Thus, the size and shape of the binding site determines which small molecules could be found as potential ligands *in silico*, especially during high-throughput rigid docking. Data were analyzed for wild soybean lipoxygenase-3 (MW 97 kDa) at 293 and 93 K and compared with the results from studies of its molecular complexes with known inhibitors, structures published by others for a derivative of the same enzyme (98 K) or a topologically close isozyme lipoxygenase-1 (at ambient temperature and 100 K). Analysis of these data allows the following conclusions. (i) Very small changes in the relative orientation of the molecules in the crystal can cause major changes in the crystal reciprocal lattice. (ii) The volume of the internal cavities can 'shrink' by several percent upon freezing even when the unit-cell and the protein molecular volume show changes of only 1–2%. (iii) Using a receptor structure determined based on cryogenic data as a target for computational screening requires flexible docking to enable the expansion of the binding-site cavity and sampling of the alternative conformations of the crucial residues.

1. Introduction

Flash-freezing has become a commonly used technique for the collection of X-ray diffraction data from frozen crystals. While freezing can help to diminish crystal decay in the X-ray beam and improve resolution, it can also stimulate changes that might effect future utilization of the results. Targeted drug design is gaining popularity as a tool to search for novel potential inhibitors of enzymes and it relies heavily on the receptor model provided by X-ray structural analysis. When the structure of the receptor site is known, high-throughput *in silico* screening allows examination of small-molecule libraries to find potential ligands that might possess some biological activity and have possible therapeutic application. Several recent publications (Edayathumangalam & Luger, 2005; Dunlop *et al.*, 2005; Halle, 2004) have discussed the pros and cons of the cryogenic technique. These authors point out that the structural changes attributed to crystal freezing can be extensive and that one may question the validity of conclusions for structures determined at temperatures of more than 200 K below their normal state. Lipoxygenases are ubiquitous enzymes in plants and mammals. The subject of our study, soybean lipoxygenase-3 (LOX-3), showed a 10% reduction in unit-cell volume and a suspiciously low data completeness

despite correct coverage of a proper part of the Ewald sphere according to the Laue symmetry. These peculiar properties prompted us to explore this phenomenon in order to seek answers as to the effect that compression of the crystal might have on the molecular structure of this globular protein with large internal cavities. The totally buried cavity in the center of the molecule's helical core was of special interest to us, since it is the binding site responsible for enzymatic activity.

Soybean LOXs are large proteins of oblate shape and consist of several domains encapsulating a mononuclear non-heme iron active site. In a redox reaction involving the iron cofactor ($Fe^{2+} \longleftrightarrow Fe^{3+}$) and molecular oxygen (hence the alternative name 'dioxygenases'), they catalyze peroxidation of unsaturated fatty acids and co-oxidation of endobiotics and xenobiotics (Kulkarni, 2001). Catalytically active systems must possess vacant coordination sites or be able to generate them in a primary dissociation step (Elschenbroich & Salzer, 1992). The soybean LOX iron cofactor is surrounded by four bound ligands (COO^- from the C-terminal Ile, three His residues bound *via* NE2) and one or two non-bound 'ligands' (Asn and H_2O or OH^-). They form a coordination sphere approximating a trigonal or tetragonal bipyramid (Skrzypczak-Jankun *et al.*, 1997, 2000, 2001, 2004; Tomchick *et al.*, 2001), with one His, Asn and H_2O showing a redox-triggered on/off coordination and much a greater mobility than the other three ligands. The typical substrate, linoleic acid, leads to an eicosanoid product, 13-hydroperoxyoctadecadienoic acid (13-HpODE), that has been localized in a metastable complex as covalently bound Enz-Fe-OO-*R* situated in the central cavity adjacent to the iron site and totally buried in the core of the molecule (Skrzypczak-Jankun *et al.*, 2001). Studying the complexes of this enzyme with various inhibitors, we have also found them in this location (Skrzypczak-Jankun *et al.*, 2000, 2004; Skrzypczak-Jankun, Zhou & Jankun, 2003; Skrzypczak-Jankun, Zhou, McCabe *et al.*, 2003; Borbulevych *et al.*, 2004). Human lipoxygenases, together with epoxy- and cyclooxygenases, are important players in inflammatory diseases and cancer, but are little understood. In the absence of structural data, our knowledge of them so far relies on modeling based on the structures of a native plant (soybean, obtained at ambient temperature, 100, 98 and 93 K) and an inhibited mammalian (rabbit, obtained at 83 K) enzyme. Our comparative studies of soybean enzymes might provide a better understanding of the structural changes imposed by crystal freezing and small-molecule binding.

2. Materials and methods

2.1. X-ray analysis

2.1.1. Crystallization. Crystals of LOX-3 (cv. Provar) were grown from 0.05 *M* sodium citrate–phosphate buffer pH 4.6, 20%(*w*/*v*) PEG 8000, 0.2% NaN_3. For data collection at cryogenic temperatures, the crystals were soaked overnight (12–15 h) in mother liquor containing 15% glycerol and flash-frozen in a cold stream of nitrogen at 93 K (Skrzypczak-Jankun *et al.*, 1996, 1997).

2.1.2. Data collection. Data collection for LOX-3 crystals at low temperature (LT) was carried out using an R-AXIS II image-plate detector and a Cu rotating-anode generator operating at 55 kV and 180 mA, with a crystal-to-detector distance of 120 mm, an oscillation angle of 1.5° and an exposure time of 30 min per frame (Skrzypczak-Jankun *et al.*, 1996). Data at ambient temperature (RT) were collected using an R-AXIS IV image-plate detector and a Cu rotating-anode

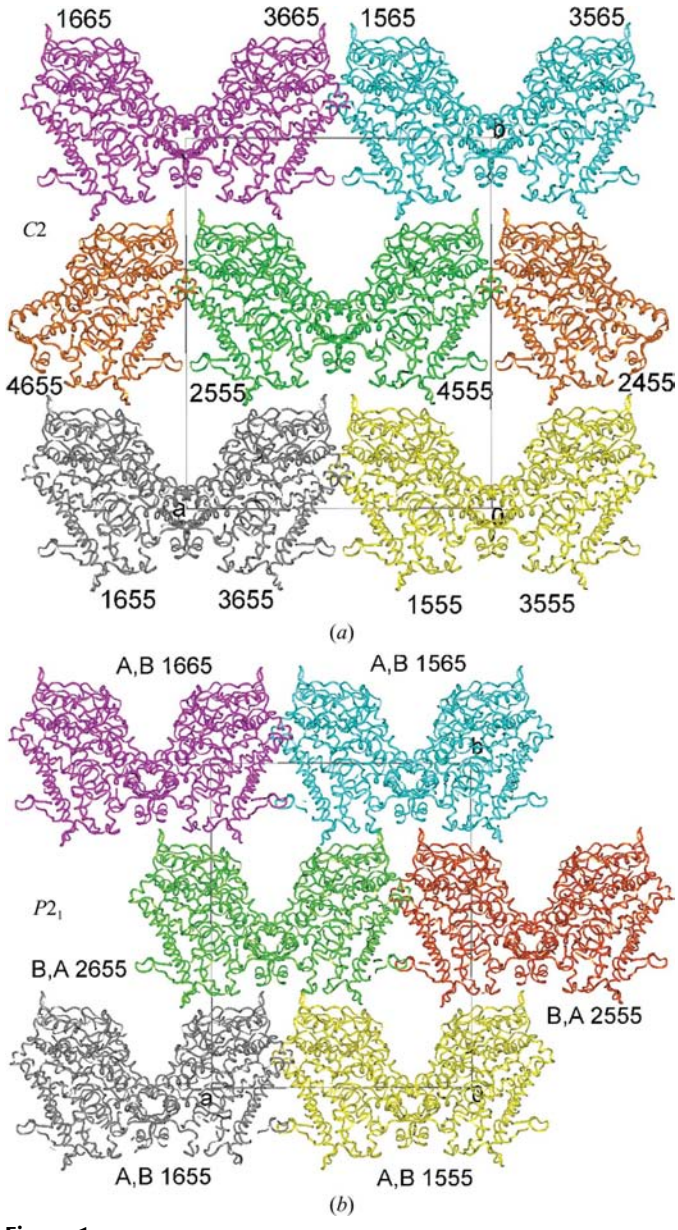

Figure 1
Packing diagrams of LOX-3 crystals viewed along the *c* axis. Only ribbons representing C^{α} backbones are shown. The gray box outlines the unit cell, with *a* horizontal and *b* vertical. (*a*) Ambient temperature (293 K), *C*2 space group, $Z = 4$; molecules 1 and 3 and molecules 2 and 4 are related by a twofold axis parallel to *b*; molecules 1 and 4 and and molecules 2 and 3 are related by a 2_1 screw axis parallel to *b*. Symmetry operators: 1555, x, y, z; 2555, $\frac{1}{2} + x, \frac{1}{2} + y, z$; 3555, $-x, y, -z$; 4555: $\frac{1}{2} - x, \frac{1}{2} + y, -z$. (*b*) 93 K, $P2_1$ space group, $Z = 4$; molecules *A* and *B* have a slightly different orientation and are no longer related by twofold symmetry; only 2_1 screw axes remain. Symmetry operators: 1555, x, y, z; 2555, $-x, \frac{1}{2} + y, -z$.

Table 1
Data-collection and refinement statistics for room-temperature (RT) and low-temperature (LT) experiments for soybean LOX-3.

Values in parentheses are for the last resolution shell.

	RT	LT	
PDB code	1rrh	1rov	1rrl
T (K)	293†	98‡	93†
Space group	$C2$	$C2$	$P2_1$
Unit-cell parameters			
a (Å)	112.7	111.0	106.4
b (Å)	137.2	136.9	133.5
c (Å)	61.8	61.5 6	0.7
β (°)	95.5	96.2	97.3
V (Å^3)	951191.0	929207.4 [2% less]	855218.4 [10% less]
Z	4	4	4 [$2A + 2B$]
Resolution limits (Å)	10.0–2.00 (2.07–2.00)	43.37–2.00 (2.13–2.00)	10.0–2.09 (2.25–2.09)
Unique reflections	53995	48034	64205
Completeness (%)	86.5 (76.7)	78 (67)	65.4§ (64.5)
R_{merge}	0.079 (0.445)	0.054 (0.217)	0.079 (0.400)
Refinement			
No. of atoms			
Protein	6790	6698	13580
Water	549	301	1064
R_{work}	0.18	0.22	0.21
R_{free}	0.23	0.23	0.31
Mean B (Å^2)			
Overall	25.93	32.80	18.84
Protein	24.34	32.39	17.66
R.m.s.d.s from ideal geometry			
Bond lengths (Å)	0.016	0.034	0.019
Bond angles (°)	1.89	3.40	2.21

† This work. ‡ Data taken from PDB entry 1rov (Vahedi-Faridi *et al.*, 2004) were used for comparison and discussion. § The low completeness is deceiving since it is a result of the true nature of this reciprocal lattice being a mixture of C and P, while completeness is calculated for P only (see Figs. 1 and 2*b*).

Table 2
Distances between the centers of protein molecules and channel dimensions in RT ($C2$) and LT ($P2_1$) LOX-3 structures.

(*a*) Distance between molecule centers.

RT		LT	
Distance	d (Å)	Distance	d (Å)
Cen_1555···Cen···3655	65	Cen_*A*_1555···Cen···*B*_1655	63
Cen_1555···Cen···3555	63	Cen_*A*_1555···Cen···*B*_1555	58
Cen_1555···Cen···4555	75	Cen_*A*_1555···Cen···*A*_2655	74
Cen_1555···Cen···2555	89	Cen_*A*_1555···Cen···*B*_2655	88
Cen_1555···Cen···2455	89	Cen_*A*_1555···Cen···*B*_2555	83

(*b*) Dimensions of the channel along c (Å).

RT	LT
74, 52	78, 44

generator operating at 50 kV and 100 mA, with a beam passing through focusing mirrors, a crystal-to-detector distance of 140 mm, an oscillation angle of 2.0° and an exposure time of 15 min per frame.

2.1.3. Structure refinement. Both structures were solved by molecular replacement using PDB code 1no3 (without water and inhibitor molecules) as a starting model with *MOLREP* from *CCP*4 v.4.2.2 (Collaborative Computational Project, Number 4, 1994). Rigid-body refinement followed by TLS refinement, as well as subsequent steps of restrained refinement with anisotropic and bulk-solvent corrections for the data, were carried out using the *REFMAC*5 program. In TLS refinement, one TLS group (residues *A*8–*A*858) and two TLS groups (residues *A*8–*A*858 and *B*8–*B*858) were used for the RT and LT structures, respectively. Once obtained, TLS parameters were included in all subsequent steps of refinement. A graphical evaluation of the model, fitting to the maps and assignment of the water molecules were performed utilizing *XtalView* (McRee, 1999). Results are summarized in Table 1. The changes in the packing of molecules and the dimensions of the crystal channels are illustrated in Fig. 1 and summarized in Table 2.

2.2. Predicting the reciprocal space of the frozen crystals based on the observed movement of the molecules

The LT phase (space group $P2_1$) can be described in a first approximation as if the two molecules, previously related by the twofold axis [non-primitive centering vector ($\frac{1}{2}$, $\frac{1}{2}$, 0)], are shifted from their original positions (RT positions). This means that new structure factors $F_{LT}(\mathbf{h})$ are related to those for RT by

$$F_{LT}(\mathbf{h}) = \exp(2\pi i\mathbf{h}\cdot\mathbf{d}_1)F_{RT}(\mathbf{h}) + \exp(2\pi i\mathbf{h}\cdot\mathbf{d}_2)F_{RT}(\mathbf{h})$$
$$= \{1 + \exp[2\pi i\mathbf{h}\cdot(\mathbf{d}_2 - \mathbf{d}_1)]\}\exp(2\pi i\mathbf{h}\cdot\mathbf{d}_1)F_{RT}(\mathbf{h}),$$

where $\mathbf{d}_1$ and $\mathbf{d}_2$ are the translations of the original basic molecular units (related by a twofold axis) to their new positions upon freezing. For the ideal RT phase $\mathbf{d}_1 = (0, 0, 0)$ and $\mathbf{d}_2 = (\frac{1}{2}, \frac{1}{2}, 0)$, the equation leads to the C-centering condition. On the other hand, for the LT phase these vectors are slightly different from the ideal values and the equation, namely its first term, makes it possible to predict the main features of the diffraction pattern. This relevant term can be rewritten into the more convenient form

$$\{1 + \exp[\pi i(h + k) + 2\pi i\Delta\ldots\mathbf{h}]\},$$

where $\Delta = \mathbf{d}_1 - \mathbf{d}_2 - (\frac{1}{2}, \frac{1}{2}, 0)$. As the difference vector in the studied case is small, there are regions where $2\pi\Delta\cdot h \simeq 2\pi n$ and $2\pi\Delta\cdot h \simeq 2\pi n + 1$. The former regions appear C-centered (strong intensities for $h + k = 2n$) and the latter regions appear as if they follow the complementary condition (strong intensities for $h + k = 2n + 1$). The reflections in between have generally uniform intensities. From the refined LT structure, we could derive a shift $\Delta = (0.0199, 0, -0.0190)$ and make the simulation based on the coordinates from RT structure analysis (Fig. 2). Calculations were performed using the

Table 3
Comparison of cavities near the iron active site in soybean LOX isozymes.

Enzyme	PDB code	R.m.s.d. CA (Å)	Cavity volumes† (Å^3) SA	CS	Inhibitor-molecule volume (Å^3)	Inhibitor name
Room temperature						
LOX-3	1rrh	Reference	55 (1)/ 60(1)	272/215		
	1no3‡ conformation *A*	0.153	70 (2)/64 (1)	317/223	123	4-Nitrocatechol
	1no3‡ conformation *B*	0.153	72 (1)/64 (1)	504/223		
	1n8q	0.133	72 (1)/58 (1)	317/211	127	Paracatechuic acid
	1hu9	0.218	86 (1)/60 (1)	358/213	135	4-Hydroperoxy-2-methoxyphenol
	1ik3	0.249	198 (1)	714	279	13-HpODE
	1jnq	0.239	198 (1)	659	252	EGC
LOX-1	2sbl	0.564	159 (1)	644		
Low temperature						
LOX-3	1rrl molecule *A*	0.469§	45 (2)/58 (1)	241/208		
	1rrl molecule *B*	0.479§	54 (1)/50 (1)	260/193		
	1rov	0.244§	54 (1)/53 (1)	278/204	¶	
LOX-1	1f8n‡ conformation *A*	0.530	56 (8)/98 (13)	237/387		
	1f8n‡ conformation *B*	0.530	80 (6)/75 (2)	319/268		

† Volumes are given for cavity 1/cavity 2. SA, probe-accessible volume from *VOIDOO*; CS, Connolly surface from *CASTp*. Center of cavity 1, *x*, *y*, *z* = 19.1, 3.9, 19.5; residues lining this cavity for LOX-3/LOX-1, Leu277/Thr259, **Gln514/Gln495**, His518/His499, Trp519/Trp500, His523/His504, Ile557/Ile538, Asn558/Asn539, Ala561/Ala542, Leu565/Leu546, Val566/Ile547, Val571/Ile552, Ile572/Ile553, Thr575/Thr556, **Phe576/Phe557**, Ile765/Ile746, **Asp766/Ser747**, Val769/Val750, **Ile770/Ile751**, Leu773/Leu754, Ile857/Ile839, Phe858/Phe840. Center of cavity 2, *x*, *y*, *z* = 18.6, −5.3, 21.5; residues lining this cavity in LOX-3/LOX-1, Val372/Val354, Ser510/Ser491, His513/His494, **Gln514/Gln495**, Phe576/Phe557, Gly715/Gly696, Gln716/Gln697, Tyr719/Tyr700, Gly720/Gly701, Ile723/Ile704, Arg726/Arg707, Thr728/Thr709, **Asp766/Ser747**, **Ile770/Ile751**. Residues in bold are at the border of two cavities. ‡ Residues with double conformations in this region: His518 in 1no3 and His499, Ile538, Ile552, Ile553, Ser747 and Val750 in 1f8n. § R.m.s.d. of 1rrl to 1rrh for all atoms, 0.816 and 0.813 Å for molecules *A* and *B*, respectively; of 1rrl molecule *B* to *A*, 0.235 Å (0.694 Å for all atoms); of 1rov to 1rrl, molecule *A*, 0.433 Å, molecule *B*, 0.450 Å. ¶ The enzyme was treated with cumene hydroperoxide (volume 151 Å^3), but its presence was not detected. Oxidation of Leu565 and Trp519 was reported, hence the OH groups at CB were removed for this comparison.

program *Jana*2000, which was specially adapted for this particular problem (Petricek & Dusek, 2000).

2.3. Evaluation of the internal cavities near the enzyme's active site

The volumes of the cavities for all compared structures were evaluated with the programs *VOIDOO* v.030312/3.3 for IRIX (Kleywegt & Jones, 1994) and *CASTp* (Liang *et al.*, 1998). All coordinates were taken from the Protein Data Bank (Berman *et al.*, 2000) as deposited, although the iron cofactor was included in all as 'atom' rather then 'heteroatom' so as not to be omitted in the calculations. The LOX-3 structure 1rrh served as a template with which all other structures were aligned using the program *ALIGN* (Cohen, 1997). The program *VOIDOO* determines the coordinates of the cavity center and gives the standard deviation for the calculated values, but the results strongly depend on the chosen grid, probe radius and orientation of the molecule. Therefore, these calculations were repeated for at least seven sets of rotated coordinates for each structure starting with following parameters: grid 0.75 Å, probe radius 1.0 Å, cavity volume accessible to probe, growth factor for van der Waals radii 1.1, grid-shrink factor 0.9, convergence criteria 0.1 Å^3 and 0.1%. The molecular volumes for enzymes were calculated with *VOIDOO* choosing a 0.45 Å grid and a probe radius of 0.5 Å, which after refinement gave a corresponding solvent content that was close to that predicted for the whole sequence by the program *Protein Calculator* v.3.2 (C. Putnam; http://www.scripps.edu/~cdputnam/protcalc.html). The volume for each inhibitor molecule was calculated using a server for calculating small-molecule properties, courtesy of Molinspiration Cheminformatics, Slovensky Grob, Slovak Republic (http://www.molinspiration.com/services/volume.html). In the case of the structures where residues were listed as 'conformer *A*' and 'conformer *B*', two sets of coordinates were prepared and calculations performed for the *A* and *B* conformers separately. The results are summarized in Table 3. The volumes of the cavities from *CASTp* are given as corresponding to the Connolly's surface, since they are easier to compare with the molecular volume of the inhibitors (calculated based on the van der Waals radii).

2.4. Docking small molecules

Known inhibitors were retrieved from the available complexes of LOX-3 (PDB codes 1no3, 1n8q, 1hu9, 1ik3 and 1jnq). These inhibitors were docked into three target structures, 1rrh (RT) and 1rrl (LT) molecules *A* and *B*, using the docking program *SLIDE* (Zavodszky *et al.*, 2002; Schnecke & Kuhn, 1999). To model induced fit upon ligand binding, *SLIDE* includes protein side chains and limited ligand flexibility (Zavodszky & Kuhn, 2005). For a more thorough sampling of the conformational space available to the ligands, low-energy conformers were generated using the program *Omega* v.1.8.1 (OpenEye Scientific Software Inc., Santa Fe, NM, USA). To test how much flexibility is needed to dock the known ligands into the active site of the room- and low-temperature LOX-3 structures, *SLIDE* parameters were changed in small step sizes, performing docking from completely rigid to increasingly flexible. The correctness of the docked ligand orientation was evaluated by calculating the root-mean-square deviation (r.m.s.d.) for the non-H atoms between the docked and the X-ray structure orientation of the same ligand. The results are summarized in Table 4.

Table 4
SLIDE parameters and corresponding r.m.s.d. values of docked ligands (all in Å).

Ligands	4-Nitrocatechol		Paracatechuic acid		4-Hydroperoxy-2-methoxyphenol		13(S)HpODE		EGC	
PDB code	1no3		1n8q		1hu9		1ik3		1jnq	
Targets	R.m.s.d.	Initial overlap	R.m.s.d.	Initial overlap	R.m.s.d.	Initial overlap	R.m.s.d.	Initial overlap	R.m.s.d.	Initial overlap
1rrh	0.00	0.30	0.04	0.30	0.39	0.30	0.41	1.00	2.10	1.20
1rrl molecule *A*	0.00	0.30	0.00	0.30	1.65	0.30	0.41	1.10	2.60	2.00
1rrl molecule *B*	0.00	0.30	0.00	0.30	0.74	0.30	1.97	1.00	2.88	1.60

3. Results and discussion

3.1. Unit cell, crystal channels and reciprocal space

A comparison of the low-temperature data for the same enzyme and crystals grown following the same protocol, 1rrl and 1rov, shows that the outcome of freezing strongly depends on crystal handling. In the first case the cryoprotectant was introduced by overnight dialysis (crystals in a 100 µl dialysis button closed with a membrane of 12 kDa molecular-weight cutoff) against the same media, but containing 15% glycerol. In the second case, glycerol was introduced gradually into the dish with the crystals, starting from 0.5% and slowly bringing it to 20% over several hours (Vahedi-Faridi *et al.*, 2004). It is a known fact that many crystals show a phase transition leading to the change of lattice and as a consequence the space group and that such changes occur at a given temperature. There are many known examples of such temperature-related phase transitions. For instance, crystals of KH_2PO_4 are monoclinic to 293 K, tetragonal below and become orthorhombic at 122 K (Falah *et al.*, 1998). Another example is the classic case of NH_4NO_3 crystals, which show five different forms, with the orthorombic form IV stable between 255 and 305 K and changing to another orthorhombic form III above 305 K, but to the tetragonal form V below 255 K (Lucas *et al.*, 1979). We have not examined the crystal structure of LOX-3 in a systematic way across the full temperature range; however, considering that the experiments (1rrl and 1rov) were 5 K apart (with the cryostat typically working at ± 1 K), it is unlikely that such a small change in temperature could be responsible for the 8% difference in the unit-cell volume (Table 1). The most probable and logical explanation could be water evaporation and a different content of glycerol in the large crystal channels (see Fig. 1 and Table 2) and molecular cavities caused by the 5% difference in the introduced amount of glycerol and the different method of cryoprotectant soaking and penetration. Our mathematical exercise of reciprocal-lattice prediction has proven that the observed phenomena (an intertwined quilted patchwork of *C* and *P* lattices; Skrzypczak-Jankun *et al.*, 1996) is a result of a small change in the relative orientation of the molecules. Namely, to simplify the description, we can view it as a shift of ~4 Å which brings closer the centers of the two molecules related by a twofold axis, with molecule *B* rotated by 7° in relation to the former twofold symmetry-related position of molecule *A*. Pictures of the simulated reciprocal space with intensities corresponding to the calculated F_{LT} structure factors compared with those found from LT diffraction show very similar features, as shown

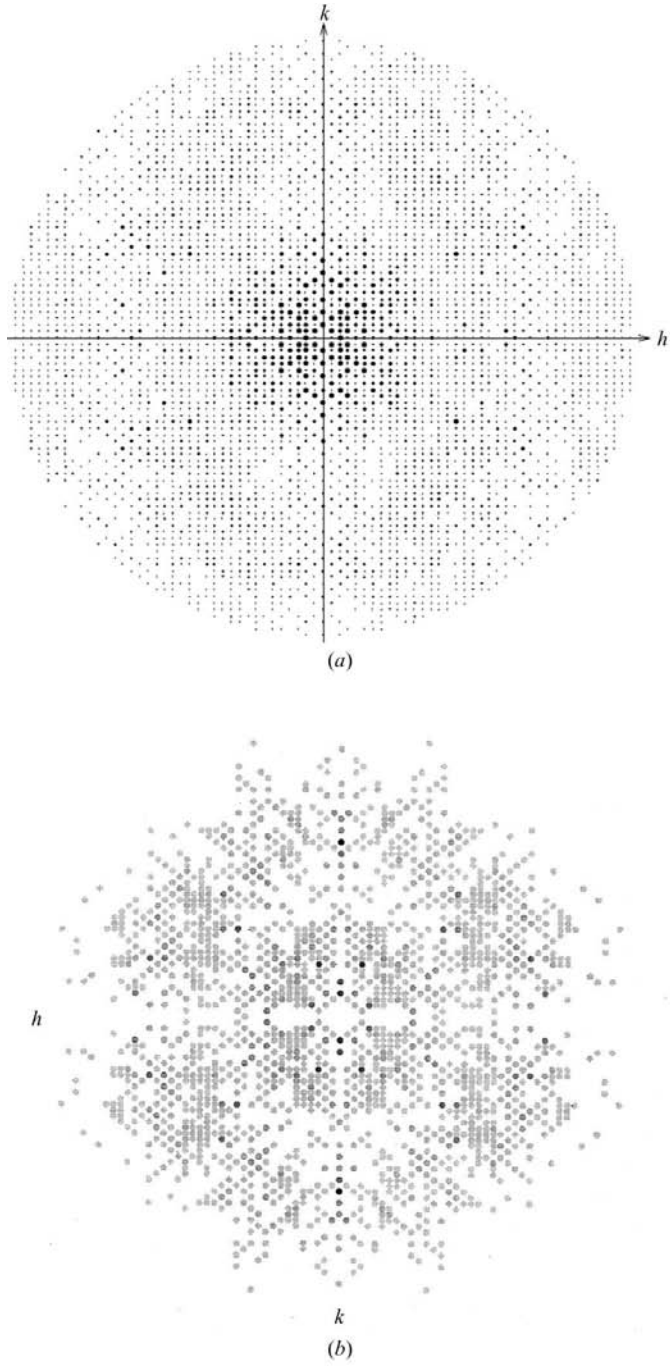

Figure 2
(*a*) Simulated roentgenograms based on theoretical calculations (*Jana*2000) and (*b*) using experimental intensities on a gray scale.

in Fig. 2. Differences in the individual calculated intensities are inevitable, since in this simulation molecules are treated as rigid bodies, solvent molecules are not accounted for and the calculations do not provide any provision for incorporating changing unit-cell parameters, solvent movement and content, surface changes or differences between two independent molecules in the asymmetric unit (the side chains, flexible loops *etc.*). Table 2 and Fig. 1 illustrate the movement of the molecules, the changing dimensions of the crystal channels and the loss of twofold symmetry in the shrunken LT LOX-3 crystal. Hence, the low completeness of the 1rrl data is a deceptive artifact that is a consequence of the true nature of the reciprocal lattice.

Usually, cryogenic conditions are chosen to provide undamaged crystals and a glassy structure for the surrounding mother liquor which is unobtrusive for diffraction. In the case of 1rrl these conditions were fulfilled. Careful examination of lipoxygenase data and several recent publications (Dunlop *et al.*, 2005; Edayathumangalam & Luger, 2005) indicated that examining the space group and the unit-cell volume [at room temperature (RT) *versus* low temperature (LT)] could be more important for preserving the crystal integrity. In the case of 1rov, the authors were familiar with previously reported LT LOX-3 data (Skrzypczak-Jankun *et al.*, 1996) and tried to avoid the phase transition leading to $P2_1$ with two molecules in the asymmetric unit. Very careful preparation of the crystals and slow gradual introduction of the cryoprotectant over a prolonged period of time allowed the preservation of the symmetry and only a slight 2% shrinkage of the unit-cell volume (Vahedi-Faridi *et al.*, 2004). Freezing turned out to be counterproductive in this case, since the goal of this experiment, the structure of LOX-3 in complex with cumene hydroperoxide, could not be achieved owing to the frequent exposure to light and prolonged soaking necessary for the cryogenic conditions. LOX forms covalent complexes with small-molecule peroxides accompanied by a color change of the sample from colorless (native LOX with Fe^{2+}) or yellowish (when the cofactor is oxidized to Fe^{3+}) to purple upon Enz-Fe-O-O-*R* formation (Skrzypczak-Jankun *et al.*, 2000, 2001; Skrzypczak-Jankun, Zhou, McCabe *et al.*, 2003, and references therein). Such complexes are highly unstable and bleach with time, with light exposure speeding up this process. Hence, the course of action taken (in the case of 1rov) may explain why the presence of the cumene peroxide complex could not be reported.

Soybean LOX-1 (839 amino acids) and LOX-3 (857 amino acids) isozymes share ∼70% homology and the same mechanism. Data for soybean LOX-1 (Table 5) also indicate a 2% reduction in unit-cell volume upon cooling to 100 K in the presence of 28% ethylene glycol (Minor *et al.*, 1994; Tomchick *et al.*, 2001). Detailed probing of various temperatures for freezing orthorhombic nucleosome crystals (193, 173, 153, 143, 138, 133 and 113 K; Edayathumangalam & Luger, 2005) shows minimal variations in unit-cell parameters and volume until 143 K, followed by an ∼5% reduction below that point. Dunlop *et al.* (2005) provide results from a similar study of tetragonal crystals of a relatively small protein of 116 residues, with three independent structure analyses at 293 K (RT) and another three at 100 K (LT). Their data show undeniably superior results at RT and a 4% (average) unit-cell volume reduction upon freezing. These crystals (LT data) were transferred to 20% glycerol + 80% precipitant solution and frozen after this single-step procedure. The original precipitant was 60% $(NH_4)_2SO_4$; hence, the transition into a cryoprotectant bath was accompanied by a reduction in the ionic strength related to the decrease in the salt concentration from 2.95 to 2.36 *M* in a mixture with glycerol. Therefore, it is not clear if the diminished performance of the crystals and the described changes in the molecular structure arise from freezing only. LOX-1 presents a similar case. The RT structure

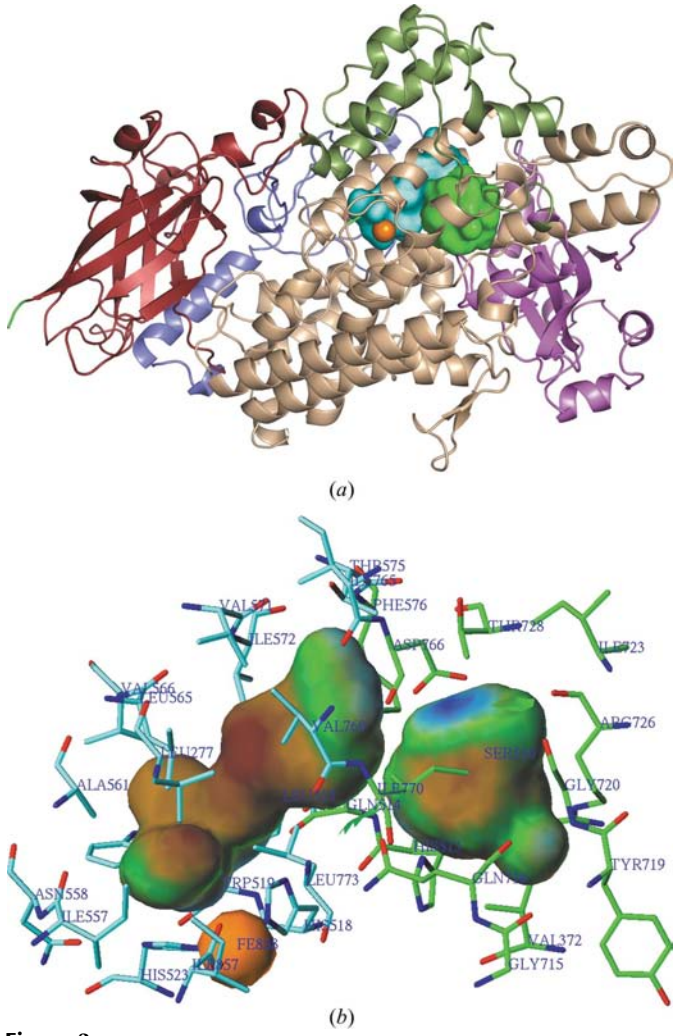

Figure 3
(*a*) Ribbon drawing of 1rrh with colors representing the subdomains according to the CATH protein structure classification; red, 'sandwich', 8–167; blue, 'irregular', 168–267; green, 'irregular', 268–355; purple, 'roll', 356–490; brown, 'up–down bundle' 491–857. Cavities 1 (cyan) and 2 (green) are represented by a surface encompassing the relevant residues and the iron cofactor is represented by an orange sphere (*PyMol* v.0.98). (*b*) Structure 1rrh as a 'stick model' showing cavities 1 (cyan bonds) and 2 (green bonds) depicted as surfaces colored according to their lipophilic potential, where brown corresponds to the highest hydrophobic area and blue to the highest hydrophilic area (*SYBYL* v.7.1; Tripos, Inc, St Louis, MO, USA).

Table 5
Comparison of unit-cell volume and solvent content.

Enzyme	PDB code	Space group	Z	Cell V (Å^3)	Matthews coefficient† (Å^3 Da^{-1})	Solvent content† (%)	Molecule V‡ (Å^3)	pH	Crystallization, cryoprotectant§
RT									
LOX-3	1rrh	$C2$	4	951179	2.46	49.9	125000 (8)	5.3	*a*
LOX-1	2sbl	$C2$	8	2139115	2.83	56.6	118100 (1)	7.0	*b*
	¶	$P2_1$	2	453342	2.40	48.8	—	5.5	*c*
LT									
LOX-3	1rrl *A*	$P2_1$	4	855218	2.21	44.3	123700 (8)	5.3	*a*, 15% glycerol
	1rrl *B*						123600 (8)		
	1rov	$C2$	4	929082	2.40	48.7	124100 (6)	5.3	*a*, 20% glycerol
LOX-1	1f8n	$P2_1$	2	445137	2.36	47.9	120200 (17)	5.5	*c*, 28% ethylene glycol

† Calculated by *Protein Calculator* based on the entire sequence. ‡ For the purpose of this comparison, the same number of residues was included in volume calculation: for LOX-3, residues 9–32 and 46–857 plus Fe, omitting one external loop; for LOX-1, residues 7–18, 32–68, 74–116, 122–453 and 461–840 plus Fe, omitting four external loops. § *a*, 0.05 *M* sodium citrate–phosphate buffer, 20% PEG 8000; *b*, 1.0 *M* ammonium acetate, 4.6 *M* sodium formate, 0.006 *M* LiCl, 0.20 *M* 2-(*N*-morpholino)-ethanesulfonic acid; *c*, 0.2 *M* sodium acetate, 9% PEG 3350. ¶ The LOX-1 structure corresponding to these conditions at RT was not deposited, but the unit cell was reported as $P2_1$, $Z = 2$, with unit-cell parameters $a = 95.6$, $b = 94.3$, $c = 50.3$ Å, $\beta = 91.3^\circ$ (Minor *et al.*, 1994).

2sbl (Boyington *et al.*, 1993) and the LT structure 1f8n (Tomchick *et al.*, 2001) are difficult to compare because of the difference in the ionic strength (6.1 *versus* 0.2), pH, composition of the mother liquor and solvent content (see Tables 3 and 5). Careful studies in an environment of controlled humidity (Juers & Matthews, 2004*a*) indicate that (i) at the optimal cryoprotectant concentration the contraction of the bulk solvent on cooling compensates for the contraction of the lattice and (ii) water transport into or out of the crystal can alter the concentration of cryoprotectant and tune the thermal contraction (especially during annealing). The authors cite an ∼1–2% shrinkage of protein molecule volume and an ∼4–5% reduction in unit-cell volume as typical for protein structures upon cooling to ∼100 K. In the case of the 1rrl structure, we have observed 10% reduction in unit-cell volume but only an ∼6% reduction in the bulk solvent, leading to a very low Matthews coefficient (Tables 1 and 5). The huge channels running parallel to the *c* axis have visibly changed their shape and volume (Fig. 1 and Table 2) and this rapid water loss may have made an impact on the molecules, which have to compensate for this.

3.2. The molecule and its inner cavities

Conclusions from analysis of biomolecular cryocrystallography (Halle, 2004) indicate that the structural models derived from such data do not portray biological macromolecules at thermodynamic equilibrium, but rather molecules trapped in local conformational and association equilibria resulting from quenching at ∼200 K, which promotes a shift toward low-enthalpy states. The glass-transition temperature for the bulk solvent is at 136 K. Hydrated proteins go through a broad glass-transition stage at 160–220 K and at ∼100 K achieve a state where all motion is effectively arrested. The solvent viscosity at this point is 10^{15}-fold higher than that of room-temperature water. It has been suggested that solvent-coupled processes, such as hydration of nonpolar cavities, protein surface, conformational switching of solvent-exposed side chains and weak ligand binding, would be affected the most and prone to cryo-artifacts. While changes on the molecular surface upon cooling have been discussed (Edayathumangalam & Luger, 2005; Juers & Matthews, 2004*b*), the influence on the internal cavities has not been well explored. In the case of LOX, it is important to study if and how cooling affects the space within the molecule, which is buried and has been designated and found to accommodate substrates and products of the enzymatic catalysis, as well as inhibitors. Fig. 3 shows the folding of the molecule (1rrh), the classification of subdomains and the two selected cavities near the iron site which participate in small-molecule binding in the LOX-3 complexes. Residues Gln514, Phe576, Asp766 and Ile770 separate these cavities and changes in their position/conformation can merge them into one space.

Despite a 10% reduction in the unit-cell volume (1rrl), the volume of the LOX-3 molecule has changed by typically only ∼1%, similarly to that in 1rov, while the summed volume of cavities 1 and 2 shows a change of ∼8%, in contrast to ∼1% in 1rov. A comparison of the cavity volumes (Table 3) shows changes between RT and LT for cavity 1 in the 1rrl molecule *A* and cavity 2 for molecule *B* and 1rov. An analysis of r.m.s.d.s (for C^α atoms only; Table 3) and a visual examination confirm that there are no significant changes either in folding or in the relative orientation of the subdomains between the RT and LT structures or between the two independent molecules in 1rrl. The average r.m.s.d.s calculated for all atoms are below 1 Å, although the differences for the individual atomic pairs can be of several angstroms. The same is true for 2sbl and 1f8n, which had quite different crystallization conditions (r.m.s.d.s of 0.374 Å for 757 CA and 0.918 Å for 6265 atomic pairs). In LOX-3 most hydrophilic side chains are affected by freezing, causing changes in the hydrogen-bonding network, salt bridges and water distribution throughout the molecule, with over 20 residues on the surface having atoms shifted by 3.6 to 9 Å in 1rrl and up to 13 Å in 1rov. No such large changes are observed inside the discussed cavities. Instead, numerous small changes are responsible for the observed differences in the volume of the cavities. With the exception of Leu277 (third

subdomain) and Val372 (fourth subdomain), the residues forming the buried cavities belong to the fifth and most sturdy subdomain. A comparison of the LT molecules *A* and *B* with their RT counterparts in this region shows that the atoms of residues Leu277 (*A*, *B*), Gln514 (*B*), His518 (*B*), Leu565 (*A*, *B*), Val566 (*A*, *B*), Val571–Ile572 and Thr575–Phe576 (*A*, *B*), lle765 (*A*, *B*), Asp766 (*A*, *B*), Ile770 (*B*), Leu773 (*A*), Ile857 (*A*), Val372 (*B*), Ser510 (*A*, *B*), Gln716 (*B*), Tyr719 (*A*, *B*), Arg726 (*B*), Asp766 (*A*, *B*) and Ile770 (*B*) have deviations of >0.5 Å. However, only Val566, Val571, Thr575, Ile765 and Ile857 (cavity 1) in molecule *A* and Val566, Ser510 and Gln716 (cavity 2) in molecule *B* show deviations of ≥1 Å, which explains why the largest changes in the cavity volume are observed for cavity 1 in molecule *A* and cavity 2 in molecule *B*. Also, it is worth noting that the residues lining these cavities (like many others throughout the structure) are engaged in hydrogen bonds stabilizing the tertiary structure, for example His518···Gln514···Gln716, Asn713···Leu773, His523···Asn558···His523, His513···Val372, and any variations might adversely affect the cavity.

Cavity 1 is mostly hydrophobic (Fig. 3*b*) and it is obvious that freezing affects its hydration, including the association of water as a possible ligand to iron. Spectroscopic data have indicated a presence of H_2O or OH^- as one of the iron ligands (Nelson, 1988). However, in the structures of wild LOX-1 or LOX-3 at RT, water was not reported (2sbl) or was assigned at a non-binding distance from iron (1rrh). The presence of bound water was found in 1no3, 1rrl *A*, 1rov and 1f8n, where it had become visible thanks to a lower thermal vibration at low temperatures (1rov, 1rrl *A*, 1f8n), shrinking space of the cavity (1rrl *A*) or restrictions imposed onto this water by engaging it in the hydrogen-bonding network (1no3, 1f8n). Therefore, changes in the position and conformation of the residues and a different distribution of the solvent explain the differences between the cavities of LT molecules *A* and *B* and LT *versus* RT in general.

A comparison of LOX in complexes indicates that the cavities' volume changes upon demand with the insertion of inhibitor (Table 3). Cumene peroxide binds to iron (Skrzypczak-Jankun *et al.*, 2000; RT experiment), forming the unstable 'purple' complex, which bleaches to oxidized LOX (reported in 1rov) and a cumene derivative, presumably its hydroxide (151 to 142 Å^3). Judging by their size, these compounds, like covalently bound iron 4-peroxy-2-methoxyphenol (1hu9) and its reduced counterpart, could be accommodated in cavity 1. The size of the cumene derivatives indicates that one might expect some noticeable cavity enlargement. However, its volume at LT is comparable to that observed in the native enzyme at RT and LT molecule *B*, suggesting the presence of the trapped water only and indicating that, in contrast to covalently bound cumene peroxide, weakly associated cumene hydroxide might have been squeezed out as a cryo-artifact.

Worth noting are changes in the cavity volumes within the same enzyme caused by the alternative conformations of one (1no3) or several residues (1f8n) (Table 3). The flexibility of His518/499 (numbering given for LOX-3/LOX-1, respectively) is extremely important, since this residue shows an ability for redox-triggered on/off coordination (Hüttermann & Kappl, 2002; Harding, 2004; Ryle & Hausinger, 2002; Wörl *et al.*, 2003; Skrzypczak-Jankun *et al.*, 2004) and together with Q514/495 could be very crucial in controlling the space availability for small molecules interacting with LOX.

3.3. Docking

Results from X-ray analysis often serve as the basis for computational docking and screening in the search for potential inhibitors. Changes imposed on the structure by flash-cooling could therefore affect the template chosen to describe the binding site. We have performed docking of known inhibitors for which the models from the X-ray analyses of the corresponding complexes were available. Both the ambient-temperature (1rrh) and the low-temperature structures (1rrl molecules *A* and *B*) were used as targets. One of the main determinants of how much flexibility should be modeled during the docking with *SLIDE* is the initial van der Waals overlap between the protein binding site and the docked ligand in its input conformation. The larger this value, the more side-chains rotations have to be employed to accommodate the ligand[1] and consequently the longer the docking process. The allowed initial overlap values used in the multiple docking runs and the resulting r.m.s.d. values of the best-docked ligands compared with their crystal structure orientations are presented in Table 4. None of the known ligands could be docked with rigid docking into any one of the three targets. This is not unexpected, since several studies have pointed out that rigid docking into the native structure targets fails to reproduce the correct complex most of the time (Erickson *et al.*, 2004; Murray *et al.*, 1999). The known ligands from PDB structures 1no3 and 1n8q (4-nitrocatechol and paracatechuic acid, respectively) are small enough to be easily accommodated by all three targets with the default side-chain flexibility parameters (initial anchor overlap 0.3 Å, initial side-chain overlap 0.3 Å). The ligand from 1hu9 (4-hydroperoxy-2-methoxyphenol) is slightly larger, so it could not be docked as closely to the X-ray structure orientation into 1rrl *A* as in 1rrh and 1rrl *B* using the default flexible parameter setting. This comes as no surprise, since cavity 1 is the smallest in 1rrl *A*, while it is about the same size in 1rrh and 1rrl *B*.

The 1jnq ligand (EGC) could not be docked correctly (r.m.s.d. ≤ 2.0 Å) into any of the structures with parameter settings that allow fast docking with *SLIDE* (initial overlap ≤ 2.0 Å, finally tolerated overlap ≤ 2.0 Å). The closest to the correct docking was achieved in 1rrh and the worst in 1rrl *B*. Even if the initial overlap was increased to beyond 2.0 Å for 1rrl *B*, no better docking could be achieved for this ligand. Docking of the 1ik3 ligand [13(S)HpODE] showed a similar trend. The closest to the correct docking with lowest initial overlap was achieved in 1rrh and the worst in 1rrl *B*. Docking the ligands 1jnq and 1ik3 into their correct binding mode

[1] The term 'ligand' when referring to docking does not mean a molecule that is covalently bound to the metal cofactor, but a small molecule that forms a molecular complex with the target.

requires flipping Gln514 out of the way to open up the narrow passage between the two cavities (Fig. 3). In addition, the backbone of residue 514 would also have to move outwards about 1.0 Å to make room for the EGC's bulky B-ring with its three hydroxyl substituents. Since *SLIDE* prefers small angle rotations of several side chains over rotating a single side chain by a large angle, this ligand was not docked correctly. The reason for the worse r.m.s.d. of the docked 13(S)-HpODE into 1rrl *B* can be found in the fact that this ligand extends deeply into cavity 2, which is the smallest in this structure. Besides the side-chain rotations modeled by *SLIDE*, the backbone of Ser510 of 1rrl *B* would have to be moved about 0.25 Å away to allow for the correct docking. These results emphasize the need to model induced fit when docking into target structures solved in the absence of bound ligands, especially when data have been obtained at cryogenic temperatures below 200 K. Modeling side-chain flexibility is imperative to achieving correct complexes. Backbone-flexibility modeling might also contribute to docking improvement and be necessary in some cases. The iron cofactor in LOX-3 easily changes the geometry of its coordination sphere from octahedral to trigonal bipyramid (Skrzypczak-Jankun *et al.*, 2004) with the C-terminal carboxylic group of Ile857 and His518 in the axial positions. This is an additional argument for making an extra allowance in the flexibility of the chosen residues when other experimental observations indicate its importance.

4. Conclusions

Comparative studies of the same proteins at different temperatures and of the native enzyme *versus* its complexes with small molecules lead to the following conclusions.

(i) The molecular structure determined from the frozen crystal may differ from that present in the native state at ambient temperature in small yet significant ways. Deviations in cryogenic structures from those determined under ambient conditions can be expected throughout the whole molecule. They should be anticipated as a transition from the dynamic disorder at RT to the 'frozen' structure at LT, whenever such a disorder or alternative structure is reasonably possible. The comparison of 1rov with 1rrl indicates that smaller change in the unit-cell volume (2% *versus* 10%) is no guarantee of better preservation of the molecular structure.

(ii) Low completeness of data does not automatically mean data omission, although the appropriateness of such a statement (considered here as '*conditio sine qua non*') has to be proven by a careful examination of the reciprocal space.

(iii) Molecules/cavities may not be equivalent to their room-temperature counterparts owing to the reduced volume caused by crystal freezing. Small-molecule binding usually induces enlargement of the binding site. In the case of lipoxygenase, an increase in the the cavity volume related to the size of the inhibitor has been observed in complexes studied at the ambient temperature. Weak inhibitors forming non-covalent molecular complexes might be 'squeezed out' by cavity compression and/or a rearrangement in its lining.

(iv) In docking calculations, flexible handling of the side-chain and main-chain atoms could be necessary, especially when the small-molecule binding occurs not in the pocket open to the molecule surface but in the buried cavities of a limited space. In the case of LOX, firstly, rigid docking to the targets obtained from structures crystallized without ligand in the binding site failed to reproduce the binding modes of known inhibitors, regardless of the RT or LT origin of the data. Secondly, larger inhibitors require opening and joining of adjacent cavities into one in order to be accommodated. Hence, rigid docking conducted without any allowance for protein movement can miss compounds that otherwise are known and good inhibitors. Therefore, one may expect meaningful results from high-throughput database searches only when there is a sufficient protein flexibility incorporated into the calculation protocol allowing the enlargement of the cavity volume and/or change in its shape. An expansion of space achieved by small changes in all cavity-lining residues may not be sufficient, when an intimate knowledge of the enzymatic structure/function points to large shifts in selected residues crucial for complex formation and catalysis.

This research was supported in part by grants from NIH (CA90524, CA109625) and the Frank D. Stranahan Endowment Fund for Oncological Research. Development of the *Jana*2000 program was supported by the Czech Grant Agency, grant No. 202/06/0757.

References

Berman, H. M., Westbrook, J., Feng, Z., Gilliland, G., Bhat, T. N., Weissig, H., Shindyalov, I. N. & Bourne, P. E. (2000). *Nucleic Acids Res.* **28**, 235–242.
Borbulevych, O. Y., Jankun, J., Selman, S. H. & Skrzypczak-Jankun, E. (2004). *Proteins*, **54**, 13–19.
Boyington, J. C., Gaffney, B. J. & Amzel, L. M. (1993). *Science*, **260**, 1482–1486.
Cohen, G. E. (1997). *J. Appl. Cryst.* **30**, 1160–1161.
Collaborative Computational Project, Number 4 (1994). *Acta Cryst.* D**50**, 760–763.
Dunlop, K. V., Irvin, R. T. & Hazes, B. (2005). *Acta Cryst.* D**61**, 80–87.
Edayathumangalam, R. S. & Luger, K. (2005). *Acta Cryst.* D**61**, 891–898.
Elschenbroich, C. & Salzer, A. (1992). *Organometallics: A Concise Introduction.* Weinheim: VCH.
Erickson, J. A., Jalaie, M., Robertson, D. H., Lewis, R. A. & Vieth, M. (2004). *J. Med. Chem.* **47**, 45–55.
Falah, C., Smiri-Dogguy, L., Driss, A. & Jouini, T. (1998). *J. Solid State Chem.* **141**, 486–491.
Halle, B. (2004). *Proc. Natl Acad. Sci. USA*, **101**, 4793–4798.
Harding, M. M. (2004). *Acta Cryst.* D**60**, 849–859.
Hüttermann, J. & Kappl, R. (2002). *Electron Paramagnetic Resonance*, Vol. 18, pp. 304–346. Cambridge: The Royal Society of Chemistry.
Juers, D. H. & Matthews, B. W. (2004*a*). *Acta Cryst.* D**60**, 412–421.
Juers, D. H. & Matthews, B. W. (2004*b*). *Q. Rev. Biophys.* **37**, 105–119.
Kleywegt, G. J. & Jones, T. A. (1994). *Acta Cryst.* D**50**, 178–185.
Kulkarni, A. P. (2001). *Cell. Mol. Life Sci.* **58**, 1805–1825.

Liang, J., Edelsbrunner, H. & Woodward, C. (1998). *Protein Sci.* **7**, 1884–1897.
Lucas, B. W., Ahtee, M. & Hewat, A. W. (1979). *Acta Cryst.* B**35**, 1038–1041.
McRee, D. E. (1999). *J. Struct. Biol.* **125**, 156–165.
Minor, W., Stec, B., Steczko, J., Axelrod, B., Bolin, J. T., Otwinowski, Z. & Walter R. (1994). *Proc. Am. Crystallogr. Assoc. Annu. Meet.* **22**, 50.
Murray, C. W., Baxter, C. A. & Frenkel, A. D. (1999). *J. Comput. Aided Mol. Des.* **13**, 547–562.
Nelson, M. J. (1988). *J. Am. Chem. Soc.* **110**, 2985–2986.
Petricek, V. & Dusek, M. (2000). *Jana*2000 *Crystallographic Computing System.* Praha, Czech Republic: Institute of Physics.
Ryle, M. J. & Hausinger, R. P. (2002). *Curr. Opin. Chem. Biol.* **6**, 193–201.
Schnecke, V. & Kuhn, L. A. (1999). *Proc. Int. Conf. Intell. Syst. Mol. Biol.*, pp. 242–251.
Skrzypczak-Jankun, E., Amzel, L. M., Kroa, B. A. & Funk, M. O. Jr (1997). *Proteins*, **29**, 15–31.
Skrzypczak-Jankun, E., Bianchet, M. A., Amzel, L. M. & Funk, M. O. (1996). *Acta Cryst.* D**52**, 959–965.
Skrzypczak-Jankun, E., Borbulevych, O. Y. & Jankun, J. (2004). *Acta Cryst.* D**60**, 613–615.
Skrzypczak-Jankun, E., Brault, P. A., Bross, R., Funk, M. O., McCabe, N. P. & Jankun, J. (2000). *American Crystallographic Association Annual Meeting*, Abstract 02.01.02.
Skrzypczak-Jankun, E., Bross, R. A., Carroll, R. T., Dunham, W. R. & Funk, M. O. Jr (2001). *J. Am. Chem. Soc.* **123**, 10814–10820.
Skrzypczak-Jankun, E., Zhou, K. & Jankun, J. (2003). *Int. J. Mol. Med.* **12**, 415–420.
Skrzypczak-Jankun, E., Zhou, K., McCabe, N. P., Selman, S. H. & Jankun, J. (2003). *Int. J. Mol. Med.* **12**, 17–24.
Tomchick, D. R., Phan, P., Cymborowski, M., Minor, W. & Holman, T. R. (2001). *Biochemistry*, **40**, 7509–7517.
Vahedi-Faridi, A., Brault, P. A., Shah, P., Kim, Y. W., Dunham, W. R. & Funk, M. O. Jr (2004). *J. Am. Chem. Soc.* **126**, 2006–2015.
Wörl, S., Hellwinkel, D., Pritzkow, H. & Kramer, R. (2003). *Chem. Commun.*, pp. 506–2507.
Zavodszky, M. I. & Kuhn, L. A. (2005). *Protein Sci.* **14**, 1104–1114.
Zavodszky, M. I., Sanschagrin, P. C., Korde, R. S. & Kuhn, L. A. (2002). *J. Comput. Aided Mol. Des.* **16**, 883–902.